sustainability

MDPI

Article

Implementing Antimony Supply and Sustainability Measures via Extraction as a By-Product in Skarn Deposits: The Case of the Chalkidiki Pb-Zn-Au Mines

Micol Bussolesi [1,*], Alessandro Cavallo [1], Vithleem Gazea [2], Evangelos Tzamos [3] and Giovanni Grieco [4]

[1] Department of Earth and Environmental Sciences, University of Milan-Bicocca, Piazza Della Scienza 4, 20126 Milan, Italy; alessandro.cavallo@unimib.it
[2] Hellas Gold Single Member S.A., Stratoni, 63082 Chalkidiki, Greece; emmy.gazea@eldoradogold.com
[3] EcoResources PC, Kolchidos Str., 3, 55131 Thessaloniki, Greece; tzamos@ecoresources.gr
[4] Department of Earth Sciences, University of Milan, Via Botticelli 23, 20122 Milan, Italy; giovanni.grieco@unimi.it
* Correspondence: micol.bussolesi@unimib.it or micol.bussolesi@gmail.com

Abstract: Antimony is one of the world's scarcest metals and is listed as a Critical Raw Material (CRM) for the European Union. To meet the increasing demand for metals in a sustainable way, one of the strategies that could be implemented would be the recovery of metals as by-products. This would decrease the amount of hazardous materials filling mining dumps. The present study investigates the potential for producing antimony as a by-product at the Olympias separation plant in Northern Greece. This plant works a skarn mineralization that shows interesting amounts of Sb. Boulangerite ($Pb_5Sb_4S_{11}$) reports on Pb concentrate levels reached 8% in the analyzed product. This pre-enrichment is favorable in terms of boulangerite recovery since it can be separated from galena through froth flotation. Boulangerite distribution in the primary ore is quite heterogeneous in terms of the inclusion relationships and grain size. However, a qualitative assessment shows that the current Pb concentrate grain size is too coarse to successfully liberate a good amount of boulangerite. The use of image analysis and textural assessments is pivotal in determining shape factors and crystal size, which is essential for the targeting of flotation parameters during separation. The extraction of antimony as a by-product is possible through a two-step process; namely, (i) the preliminary concentration of boulangerite, followed by (ii) the hydrometallurgical extraction of the antimony from the boulangerite concentrate. The Olympias enrichment plant could therefore set a positive example by promoting the benefits of targeted Sb extraction as a by-product within similar sulfide deposits within the European territory.

Keywords: critical raw materials; antimony; Greece; strategic mineral resources; Pb-Zn-Au deposits; by-product

Citation: Bussolesi, M.; Cavallo, A.; Gazea, V.; Tzamos, E.; Grieco, G. Implementing Antimony Supply and Sustainability Measures via Extraction as a By-Product in Skarn Deposits: The Case of the Chalkidiki Pb-Zn-Au Mines. *Sustainability* **2024**, *16*, 8991. https://doi.org/10.3390/su16208991

Academic Editor: Rajesh Kumar Jyothi

Received: 13 September 2024
Revised: 10 October 2024
Accepted: 14 October 2024
Published: 17 October 2024

1. Introduction

1.1. Antimony Overview

Antimony (Sb) is one of the elements listed as a Critical Raw Material (CRM) by the European Union [1] but it is also considered critical by other countries as well, such as Australia, Russia, the UK and the USA [2]. Even China, the main antimony supplier, is expecting an increase in its criticality [3]. Antimony is also considered one of the world's scarcest metals [4], and this is reflected in peak prices due to shortages of ore supply and/or increases in demand during certain historical periods (e.g., increases in Sb production for military applications during periods of war). An assessment by Henckens et al. [4], however, concludes that considering the overall trend, there is no significant correlation between its price and its geological scarcity, making Sb supply in the future uncertain. At the same time, a more recent resilient approach by van den Brink et al. [5] states that if EU wants to reduce

its import dependency (currently based on Turkey, Bolivia and China as the main suppliers), the extraction of Sb, as well as the capacity for its processing, in the European territory must be enhanced. The wide use of Sb dates back to the 1900s, when the Russian–Japanese war triggered its demand for the production of ammunition. More recent applications include the use of Sb as a flame retardant (antimony trioxide—ATO); in electronics, plastics, fabrics, aircrafts and vehicle covers; as a catalyst for plastic production (especially polyethylene terephthalate—PET); and for use in diodes production in electronics and lead–antimony batteries [6].

The main Sb world resources are located in Australia, Bolivia, Myanmar, China, Mexico, Russia, Turkey and Tajikistan [7]. Within the European territory, Sb occurrences have been reported in France, Germany, Sweden, Finland, Slovakia and Greece, but they are not currently considered to be of economic interest [8]. The main world Sb producer is China, which recently imposed an export tax on antimony ores and concentrates and decreased its internal production, thereby increasing the supply risk of Sb [8]. For these reasons, Sb was still considered critical in the EU's 2023 report on Critical Raw Materials [1]. Antimony is mainly used: (i) as a flame retardant, where ATO is commonly used as a flame retardant in plastics, textiles and other materials to prevent or delay the spread of fire; (ii) as an alloying agent, where Sb is added to other metals such as lead, tin and copper to improve their hardness and strength; (iii) in batteries, where Sb is used in the production of lead–acid batteries as an alloying element to enhance their performance; (iv) in the semiconductor industry, where Sb is used to make transistors and diodes; (v) in the glass industry, where Sb is used as a fining agent in the production of glass to remove bubbles and improve clarity; (vi) as pigments, where Sb compounds are used in paints, ceramics and plastics; (vii) in military applications, for use in the production of night vision goggles, explosive formulations, flares, nuclear weapons, infrared sensors and tracer bullets.

One of the reasons for the lack of Sb extraction in the EU is the strict legislation that some countries have on the matter, as this element is potentially harmful to human health. Exposure to high levels of antimony can cause a variety of negative effects on health, including respiratory issues, skin irritation and gastrointestinal problems as well as damage to the liver, kidneys and heart. ATO is classified by the EU as "suspected of causing cancer via inhalation" according to Regulation (EC) 1272/2008.

From most products, such as fire retardants (ATO), Sb compounds cannot be recycled because they are dissipated through use, although the recycling of PET containers does make an indirect contribution. However, Sb can be recovered from most applications where it has been used as an additive in lead alloys. Secondary Sb (mostly derived from recycled lead–acid batteries) is a significant source of supply in many countries, totaling approximately 40,000 tons per year and accounting for about 20 per cent of the total Sb used. The use of Sb in lead–acid batteries may be significantly reduced in the future as alternative vehicle technologies are increasingly adopted worldwide.

Antimony enrichments in Greek ore deposits have been preliminary investigated by [9,10] and Bussolesi et al. [11]. Stibnite (Sb_2S_3), boulangerite ($Pb_5Sb_4S_{11}$), bournonite ($PbCuSbS_3$), berthierite ($FeSb_2S_4$) and valentinite (Sb_2O_3) have been detected in mineralization at the Stratoni plant [10], but their behavior and possible recovery from this working enrichment plant is still unknown. The aim of this work was to investigate the possibility of exploiting the extraction of antimony as a by-product during lead–zinc–gold production by studying the processing of Sb at the Stratoni flotation plant as well as its texture and mineralogy in the primary ore. The recovery of a Critical Metal as a by-product would simultaneously decrease its content in mining dumps and tailings and would partially address the increasing demand for antimony in the world market. In other words, this method would effectively provide a new and sustainable source for a scarce metal while recovering it from dumps and therefore decreasing its hazardous effects on the environment at the same time.

1.2. Geological Framework

The Kassandra district is located in the northeastern part of the Chalkidiki peninsula in Northern Greece. It is part of the Serbo–Macedonian Massif, divided into the Vertiskos and Kerdyllon units [12]. The Au–Cu porphyry and Au–Ag–Pb–Zn–Cu carbonate replacement ore deposits are situated in the Kerdyllon unit, associated with granitic and granodioritic intrusions (Eocene to Oligocene in age) that are emplaced in poly-deformed metamorphic basement rocks [9]. The district comprises different sulfide deposits, from north to south: Olympias, Piavitsa, Stratoni (divided into Mavres Petres and Madem Lakkos) and Skouries (Figure 1a).

Stratoni and Olympias, located on the footwall of the Tertiary Stratoni fault, are the two main carbonate replacement massive sulfide Pb–Zn (Ag–Au) deposits in the district. Sulfide mineralization occurs within the amphibolite-grade metamorphic rocks (including marbles), an assemblage that represents a metamorphosed marine sedimentary–volcanic sequence from the Mesozoic age [13]. Antimony occurrences have been detected in these mixed sulfide ore deposits, which are currently being operated by Hellas Gold S.A./Eldorado Gold.

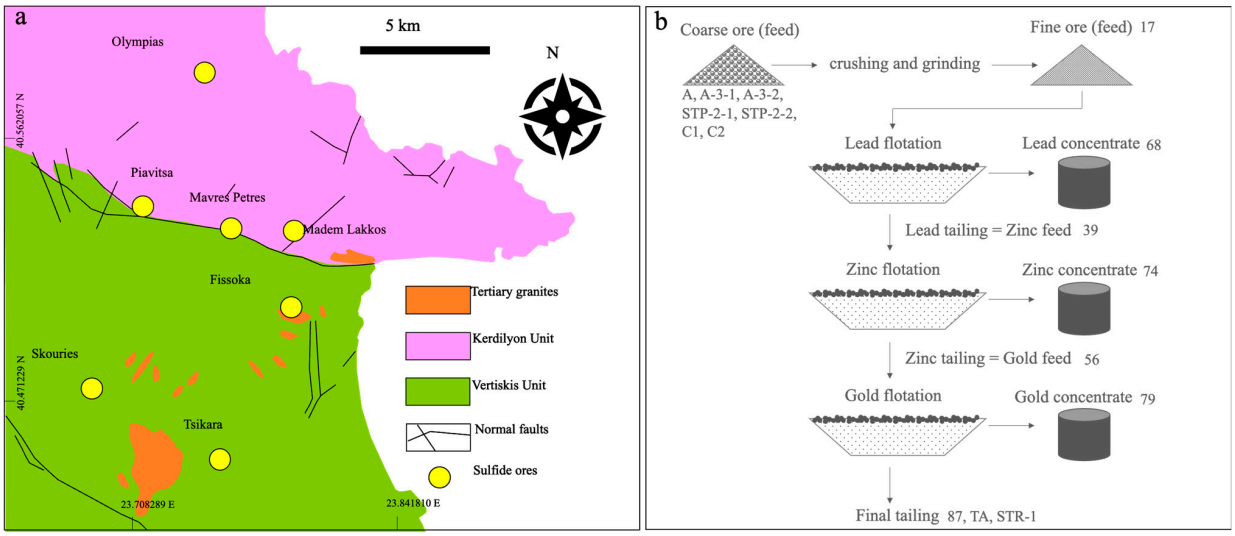

Figure 1. (**a**) simplified geological map of the Kassandra mining district; modified after Högdahl et al. [14]; (**b**) simplified flotation plant; sample tags are reported as numbers.

1.3. Flotation Enrichment Plant

In the past, both the Olympias and Stratoni enrichment plants were active, but nowadays only the Olympias one is in operation.

The plant currently produces three concentrates: galena, sphalerite and pyrite/arsenopyrite, which are then sent for metallurgical treatment for the recovery of Pb, Zn and Au, respectively. The separation of minerals through flotation involves the use of chemicals to selectively separate these minerals based on their surface properties. The minerals are first crushed and ground into a fine powder, which is then mixed with water and chemicals called reagents. The reagents used in flotation depend on the type of minerals being separated, but these typically include collectors, frothers and modifiers. Collectors are chemicals that selectively bind to the target mineral, frothers help to create a stable foam layer on the surface of the flotation cell and modifiers are added to adjust the pH or other properties of the slurry to optimize the flotation process.

The Olympias flotation plant works in three consecutive circuits, enriching galena first, then sphalerite and finally the gold-rich pyrite–arsenopyrite (Figure 1b).

2. Materials and Methods

2.1. Samples

Samples were collected from the Olympias flotation plant, which enriches the ores collected from the Olympias and Stratoni mines. The collected samples were classified as feed representative samples (centimetric ore pebbles) and samples from different stages of the flotation plant (flotation sands) (as shown in Table 1).

Table 1. Sample tags, type of sampled material and locations.

Sample	Type	Location	Comment
A-5	ore	Mavres Petres (Stratoni)	Coarse ore
A-3-1	ore	Madem Lakkos (Stratoni)	Coarse ore
A-3-2	ore	Madem Lakkos (Stratoni)	Coarse ore
STP-2-1	ore	Madem Lakkos (Stratoni)	Coarse ore
STP-2-2	ore	Madem Lakkos (Stratoni)	Coarse ore
C1	ore	Stratoni	Coarse ore (sulfide-rich)
C2	ore	Stratoni	Coarse ore (gangue-rich)
17	flotation	Olympias Plant	Feed before Pb flotation
39	flotation	Olympias Plant	Pb-tailing–Zn feed
56	flotation	Olympias Plant	Zn-tailing–Au feed
68	flotation	Olympias Plant	Pb concentrate
74	flotation	Olympias Plant	Zn concentrate
79	flotation	Olympias Plant	Au concentrate
87	flotation	Olympias Plant	Final tailing
TA	flotation	Olympias Plant	Final tailing
STR-1	flotation	Stratoni Plant	Final tailing

2.2. Grain Size Analysis

Grain size analysis was performed on concentrates and tailings from the flotation plant. The sieving process was performed with mesh sizes of 1 mm, 0.5 mm, 0.250 mm, 0.125 mm, 0.063 mm and 0.038 mm.

2.3. Whole Rock Analyses (XRF, ICP-MS)

XRF analyses were performed on pressed fine powder pellets, with a Panalytical Epsilon 3XL spectrometer equipped with an X-ray tube with a 50 μm window and a Rh anode with a power up to 9 W. The instrument operates with a programmable voltage between 4 and 50 kV with 0.01 kV steps, and a current between 1 and 1000 μA with 1 μA steps. The emission lines were simultaneously counted through a multichannel MCA. The raw data were analyzed through Software Epsilon 3-XL using the Omnian standardless model. The results are to be considered semi-quantitative.

ICP-MS analyses were performed at the ActLabs laboratory in Canada through the Aqua Regia Ultratrace 1 program.

2.4. Mineralogy (XRPD, Optical Microscopy)

XRPD analyses were performed at the University of Milan with a PANalytical X'Pertpro instrument set at the following operating conditions: 40 kV of voltage; 40 mA of current; and Cu anticathode Kα1/Kα2: 1.540510/1.544330 Å. Data were elaborated with the X'Pert Highscore v.2.3 software.

The qualitative XRPD analysis was performed running the PANalytical X'Pert High-Score Plus 2.1.0 software, using the ICSD PDF2 database. A semi-quantitative evaluation of the relative abundance of single minerals was obtained with the internal standard technique (by adding 20 wt.% of corundum powder) and the reference intensity ratio (RIR) method. This approach is based on a least squares minimization approach, like the Rietveld method. However, this method is not recommended for use on minerals with high structural disorder, like phyllosilicates (such as micas, chlorite, serpentine and clay minerals). The abundances were cross-checked with XRF data for the sulfides, with a good

agreement except for the sphalerite content of sample 74. The high discrepancy detected for sphalerite in this sample could be due to peak overlap, fluorescence effects or the preferential orientation of the X-ray diffraction.

2.5. Mineral Chemistry (SEM, EMPA)

Preliminary SEM analyses were conducted at the University of Milano–Bicocca using a Tescan (Tescan Orsay Holding, Brno, Czech Republic) VEGA TS 5136XM equipped with an EDS detector.

Mineral chemistry was determined using a JEOL 8200 electron microprobe (JEOL Ltd., Akishima, Japan) equipped with a wavelength dispersive system (WDS) at the Earth Sciences Department of the University of Milan. The microprobe system operated using an accelerating voltage of 15 kV, a sample current on brass of 15 nA and a counting time of 20 s on the peaks and 10 s on the background. A series of natural minerals was used as standards for the analyses.

3. Results

3.1. Grain Size

An analysis of the grain sizes of the concentrates and the tailings (Figure 2) reveals that the feed was crushed and grinded to a relatively uniform grain size. Of the three concentrates, the lead one was the most coarse, with a D90 of 400 µm (=90% of the grains were smaller than 400 µm), while the zinc and gold concentrates showed a D90 of 127 µm and 240 µm, respectively. The two tailings showed very similar grain sizes, showing a D90 of 620 and 700 µm, respectively.

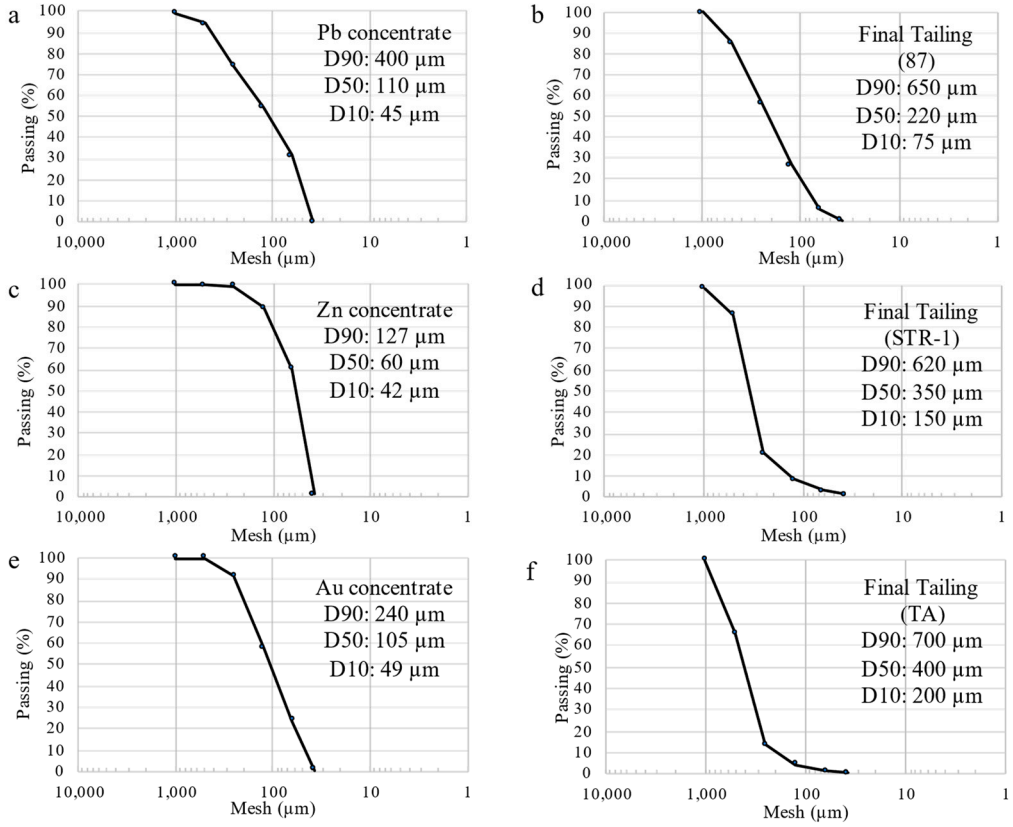

Figure 2. Grain size distribution of Pb (**a**), Zn (**c**) and Au (**e**) concentrates and of the different final tailings (**b**,**d**,**f**) produced during the flotation process.

3.2. Optical Microscopy

The ore mineral assemblage comprised galena (PbS), sphalerite ((Zn,Fe)S), pyrite (FeS_2) and arse–nopyrite (FeAsS) (Figure 3a). The subordinate phases were boulan-

gerite ($Pb_5Sb_4S_{11}$), bournonite ($PbCuSbS_3$), chalcopyrite ($CuFeS_2$), pyrrhotite ($Fe_{1-x}S$) and graphite (C) (Figure 3b,c). The most abundant mineralogical phase was pyrite, which formed large (200–1000 µm) subhedral to anhedral crystals. Sphalerite and galena also formed subhedral crystals, with grain size variables from the micrometric to the millimetric. Sphalerite often showed tiny chalcopyrite grains, commonly known as "chalcopyrite disease", as well as local Sb-rich galena inclusions (Figure 3a). Arsenopyrite formed rhombus-shaped euhedral crystals of up to 100 µm in size (Figure 3b). Boulangerite occurred as long acicular crystals either within galena (Figure 3b), within the matrix or within the massive pyrite (Figure 3c). Rare bournonite (20–30 µm) was found in association with boulangerite, including in the pyrite (Figure 3c). Chalcopyrite was not abundant and formed tiny crystals within the matrix and anhedral blebs associated with the pyrite (Figure 3d) or tiny grains within the sphalerite. Pyrrhotite was locally abundant, and formed anhedral aggregates in association with pyrite, galena and chalcopyrite (Figure 3d). Graphite, found only locally, formed crystals with a "flakey" habit.

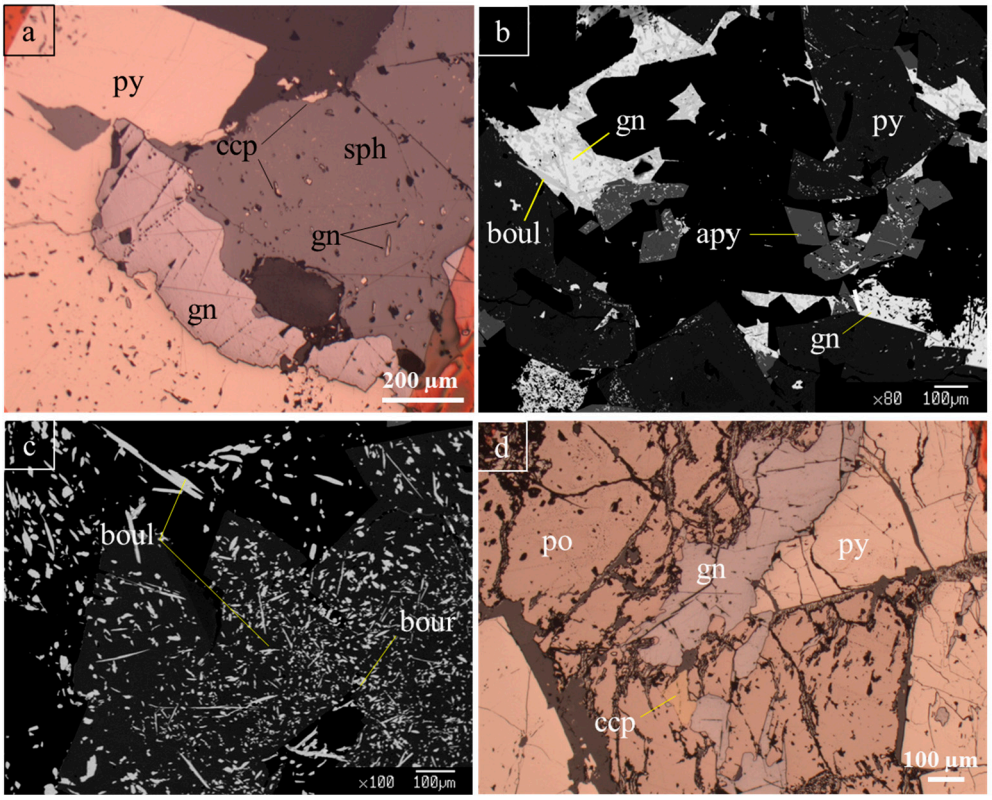

Figure 3. Texture and optical features of Stratoni ore minerals; (**a**) pyrite, galena and sphalerite with chalcopyrite disease (optical microscope reflected light); (**b**) boulangerite replacing galena and arsenopyrite (BSE image); (**c**) acicular boulangerite crystals within carbonate gangue and arsenopyrite (BSE image); (**d**) pyrrhotite, pyrite, chalcopyrite and galena crystals (optical microscope, reflected light).

3.3. X-Ray Diffraction Mineralogy

Representative samples from the crushed and grinded ores were mainly composed of quartz, dolomite, calcite and minor muscovite, gypsum and pyrite. Galena, sphalerite and boulangerite were too scarce to give a detectable diffraction peak (Figure 4a). After the first flotation circuit, the resulting materials were the Pb concentrate, mainly composed of galena (33.48%), quartz (32.93%), pyrite (12%) and minor boulangerite (7.79%) (Figure 4b). A tailing reporting to the second flotation circuit comprised abundant quartz (37%), calcite (14%), dolomite (15%), gypsum (6.02%), muscovite (13%), pyrite (11%) and minor sphalerite (3.6%) (Figure 4c). The second flotation circuit produced a Zn concentrate (sphalerite 71.85%, pyrite 23% and minor galena 3.15%) (Figure 4d), and a tailing reporting to the third

flotation circuit, composed of quartz (45%), dolomite (12%), calcite (14%), muscovite (14%) and minor gypsum and pyrite (Figure 4e). The third and last flotation circuit produced an Au concentrate (pyrite 53% and arsenopyrite 19%, with quartz 23%, Figure 4f) and a final tailing with abundant quartz (34.3%), dolomite (30.3%), calcite (17.2%) and minor muscovite (15.2%) and gypsum (3%) (Figure 4g).

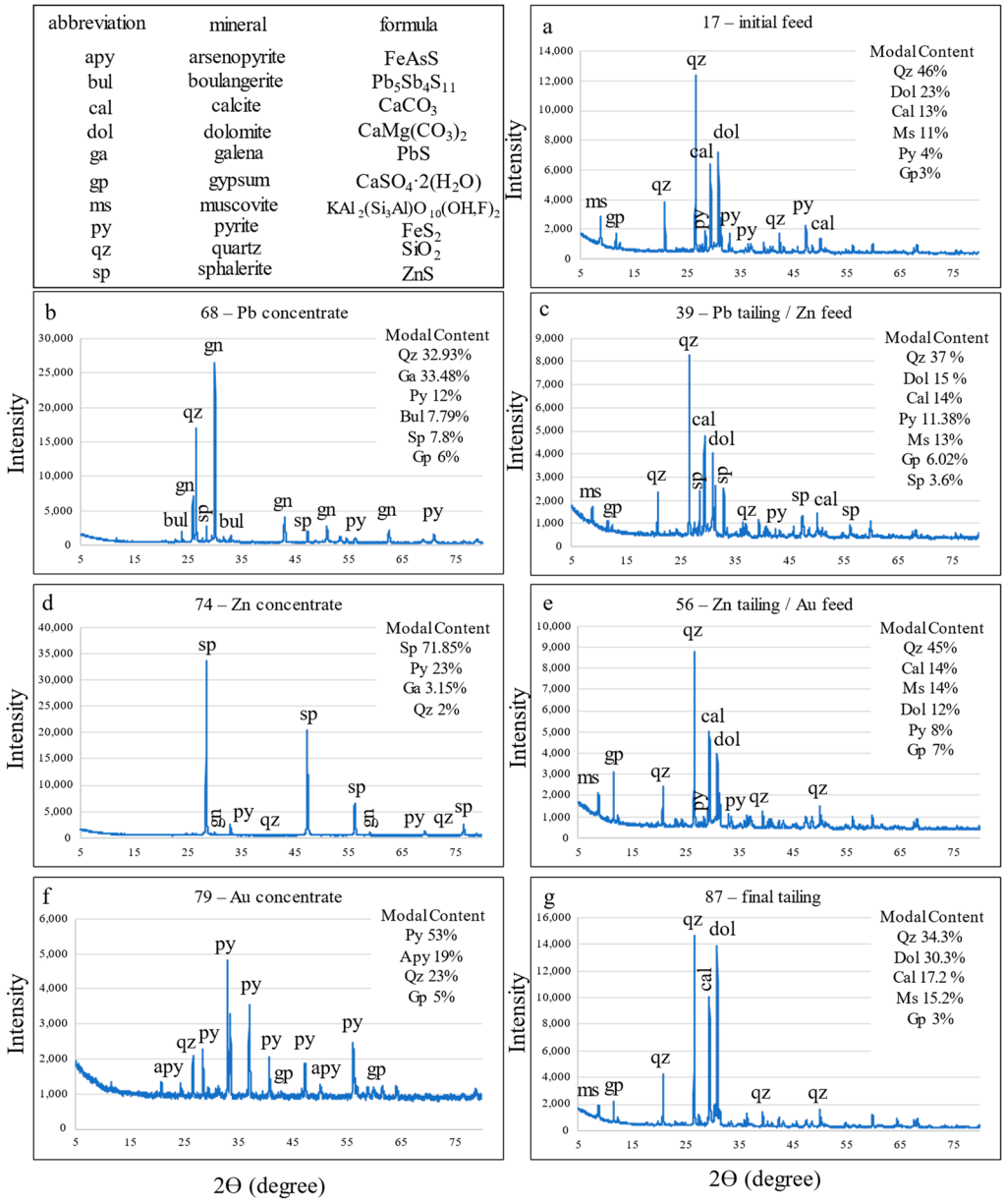

Figure 4. XRD patterns and mineral modal contents (relative abundance %) of initial feed (**a**) Pb concentrate; (**b**) Pb tailing acting as Zn feed (**c**); Zn concentrate; (**d**) Zn tailing acting as Au feed; (**e**) Au concentrate; (**f**) final tailing (**g**).

3.4. Mineral Chemistry

The average major and minor element composition of the mineralogical phases in the Stratoni ores is reported in Table 2. Galena showed a variable amount of Pb (82.15–86.98 wt%) and some enrichments in minor elements, such as W (up to 0.54 wt%), Bi (up to 0.42 wt%) and Sb (up to 2.82 wt%). Remarkably, the Ag content in galena was mostly below the detection limit. The analyzed crystals were almost stoichiometric, with Pb = 1 apfu (atoms per formula unit), S = 0.98 apfu and Sb = 0.01 apfu. Pyrite showed quite a homogeneous major element composition (Fe 45.59–47.27 wt%) and had important

enrichments in some minor elements, such as As (up to 3.46 wt%), Mo (up to 0.67 wt%), Pb (up to 0.49 wt%), Zn (up to 0.71 wt%) and Sb (up to 0.44 wt%). The crystals showed on average the following mineral formula: $Fe_{1.02}S_{1.95}$. Sphalerite showed quite a variable major element composition, with Zn (53.46–59.11 wt%) and Fe (5.63–12.84 wt%), and had an enrichment in Mo (up to 0.47 wt%), Cd (up to 0.36 wt%) and Cu (up to 0.44 wt%). This variability is reflected in the atoms per formula unit, with Fe (0.10–0.22), S (0.98–1.00) and Zn (0.79–0.89), using the following mineral formula (on average): $(Zn_{0.84}Fe_{0.16})S_{0.99}$. Arsenopyrite showed a homogeneous major element composition, with As (40.80–42.97 wt%) and Fe (35.82–36.31 wt%), and some enrichments in W (up to 0.41 wt%). Atoms per formula unit showed As (0.85–0.91), homogeneous Fe (1.01–1.02) and S (1.07–1.13), with an average formula of $Fe_{1.01}As_{0.87}S_{1.11}$, indicating a replacement of As by S. Boulangerite showed a homogeneous major element composition, with Pb (54.63–55.84 wt%) and Sb (25.64–26.45 wt%), and had minor element enrichments in As (up to 0.37 wt%) and Zn (up to 3.52 wt%). Atoms per formula unit showed Pb (4.84–5.12), Sb (3.86–4.16), As (0.06–0.10) and S (10.01–10.73), with an average formula of $Pb_{5.04}Sb_{4.}07As_{0.08}S_{10.52}$. Bournonite was rare as only two grains were detected and analyzed. They showed homogeneous major element composition and had minor As enrichments (0.46–1.63 wt%). Atoms per formula unit showed Pb (1.00), Cu (0.99–1.02), Sb (0.94–1.03) and S (2.93–2.94), with an average formula of $Pb_{1.00}Cu_{1.00}Sb_{0.99}S_{2.93}$. Chalcopyrite was not widespread, but the detected and analyzed crystals showed rather homogeneous major element composition (Fe 29.11–30.56 wt% and Cu 33.10–34.27 wt%). All the crystals, moreover, showed slight enrichments in Mo (up to 0.39 wt%). Atoms per formula unit showed Cu (0.97–1.01), Fe (0.97–1.02), S (1.95–1.99), with an average formula of $Cu_{1.00}Fe_{1.00}S_{1.97}$. Pyrrhotite showed homogeneous Fe (59.72–60.65 wt%) amounts, and had minor enrichments in Mo (up to 0.53 wt%). Atoms per formula unit showed Fe (0.94–0.95) and S (1.04–1.05), with an average formula of $Fe_{0.94}S_{1.05}$.

Table 2. Sulfide mineral chemistry (average); bdl: below detection limit.

	Galena	Pyrite	Sphalerite	Arsenopyrite	Boulangerite	Bournonite	Chalcopyrite	Pyrrhotite
wt%	**(n = 20)**	**(n = 40)**	**(n = 12)**	**(n = 8)**	**(n = 6)**	**(n = 2)**	**(n = 5)**	**(n = 6)**
As	bdl	0.70	bdl	41.62	0.31	1.04	bdl	bdl
Fe	0.13	46.66	9.14	36.01	0.17	bdl	29.93	60.27
S	12.93	51.34	32.74	22.65	17.85	19.04	33.76	38.42
Mo	bdl	0.52	0.37	0.25	bdl	bdl	0.34	0.47
W	0.11	0.07	bdl	0.15	0.14	0.14	bdl	0.13
Pb	85.52	0.22	0.15	0.11	55.22	42.06	0.12	0.13
Ag	0.05	bdl	bdl	bdl	bdl	bdl	0.05	0.04
Bi	0.21	0.20	0.13	0.11	0.18	0.12	0.18	0.17
Cd	bdl	bdl	0.17	bdl	bdl	bdl	bdl	bdl
Zn	0.02	0.05	56.76	bdl	0.63	bdl	0.61	0.03
Sb	0.32	bdl	bdl	0.04	26.23	24.30	bdl	bdl
Cu	0.05	0.04	0.08	bdl	0.04	12.91	33.78	0.07
tot	99.42	99.93	99.67	101.08	100.88	99.66	98.92	99.84
a.p.f.u.								
As	0.00	0.01	0.00	0.87	0.08	0.07	0.00	0.00
Fe	0.01	1.02	0.16	1.01	0.06	0.00	1.00	0.94
S	0.98	1.95	0.99	1.11	10.52	2.93	1.97	1.05
Mo	0.00	0.01	0.00	0.00	0.00	0.00	0.01	0.00
W	0.00	0.00	0.00	0.00	0.01	0.00	0.00	0.00
Pb	1.00	0.00	0.00	0.00	5.04	1.00	0.00	0.00
Ag	0.00	0.00	0.00	0.00	0.00	0.00	0.00	0.00
Bi	0.00	0.00	0.00	0.00	0.02	0.00	0.00	0.00
Cd	0.00	0.00	0.00	0.00	0.00	0.00	0.00	0.00
Zn	0.00	0.00	0.84	0.00	0.18	0.00	0.02	0.00
Sb	0.01	0.00	0.00	0.00	4.07	0.99	0.00	0.00
Cu	0.00	0.00	0.00	0.00	0.01	1.00	1.00	0.00

3.5. Whole Rock Analyses

Whole rock compositions were consistent with the x-ray diffraction results of the flotation plant samples in terms of major and minor metals (Table 3). The initial feed was enriched mainly in S, Fe_2O_3 and MnO, with minor Zn, As and Pb enrichments. The first flotation circuit produced a concentrate rich in galena (Pb 29.2 wt%), sphalerite (Zn 5.01 wt%) with a minor presence of Sb (2.06 wt%). The tailing, serving as a feed for the second flotation circuit, was again enriched in S, Fe_2O_3 and MnO, with a minor presence of Zn and As. The second flotation circuit produced a sphalerite concentrate (Zn 26.94 wt%) with Cd enrichments (>2000 ppm) and a tailing served as the feed of the third flotation circuit, which was rich in S and Fe_2O_3 as major metals. The third flotation circuit produced an Au concentrate in the form of pyrite (Fe_2O_3 20.96 wt%) and arsenopyrite (As 4.11 wt%), and the final tailing, once again was rich in S, Fe_2O_3 and MnO but deprived of Pb, Zn and Sb.

Table 3. Metal composition (wt% or ppm) of feed, concentrates and tailings of the Olympias flotation plant.

	17—Initial Feed	68—Pb Concentrate	39—Pb Tailing Zn Feed	74—Zn Concentrate	56—Zn Tailing Au feed	79—Au Concentrate	87—Final Tailing	STR-1—Tailing
S (%)	3.41	7.49	3.92	14.88	3.20	10.43	2.34	9.18
MnO (%)	6.14	0.98	6.02	0.57	5.96	0.54	4.16	0.93
Fe_2O_3 (%)	7.96	9.19	8.02	9.75	8.03	20.96	3.17	19.98
Cu (ppm)	681	11,479	493	2880	644	610	149	98.4
Zn (%)	2.16	5.01	2.34	26.95	0.39	0.55	0.30	0.35
As (%)	1.61	0.77	1.73	0.21	1.93	4.12	0.43	1.82
Sb (%)	0.12	2.06	0.03	0.12	0.03	0.03	0.03	0.02
Pb (%)	0.99	29.2	0.37	1.08	0.30	0.50	0.21	0.25
Bi (ppm)	0.87	47.9	0.26	1.64	0.24	0.42	0.14	0.09
Sc (ppm)	1.10	0.3	1.2	bdl	1.1	0.4	1.3	0.8
Ga (ppm)	6	10.5	6.02	59.7	2.08	2.53	2.22	0.7
Mo (ppm)	5.17	3.01	3.26	1.34	2.47	1.46	2.68	0.83
Ag (ppm)	31.1	>100	11.9	79.9	5.75	17.6	3.21	8.65
In (ppm)	1.06	3.25	1.11	20.8	0.19	0.57	0.12	0.2
Cd (ppm)	137.3	401.2	152	>2000	22.6	70.6	13.2	17.1

4. Discussion

The current risk in the supply of critical raw materials has led to enhanced efforts to reduce such criticality through different actions, among which has been not only been the evaluation of reopening several abandoned mining sites and the recovery of valuable CRMs from waste and tailing dumps, but also the potential for recovering CRMs as by-products from working enrichment plants [1].

The flotation processes at Stratoni work in three circuits, concentrating galena first, then sphalerite and finally Au-bearing pyrite–arsenopyrite. The analyses on the three concentrates showed that Sb, Bi and Ag mostly report to the galena concentrate. The sphalerite concentrate shows the highest Cu, Ga, In and Cd enrichments and the pyrite–arsenopyrite concentrate shows an As enrichment. Mo is quite evenly distributed among all the products, from feed to tailing, implying that it is not enriched in any of the flotation stages. Bi and Ag enrichments in galena agree with studies in the literature [15,16], as well as Cd and Ga enrichments in the sphalerite product [17,18].

The most promising result for the potential recovery of CRMs concerns the Sb enrichment in the galena concentrate. The amount of Sb (2.06 wt%) detected in the Pb concentrate cannot be explained solely by the Sb enrichments in galena—which was up to 2.82 wt% in a single analysis, probably due to undetected boulangerite micro-inclusions, but 0.32 wt% on average for all the analyzed crystals—and is mostly due to the presence of boulangerite and minor bournonite in the concentrate. This picture makes the Sb recovery as a by-product of

the galena concentrate a viable process as most of the Sb is stored in Sb mineral phases that can potentially be separated through flotation.

Recent studies have reported the presence of Sb-bearing mineralogical phases in the ores of the Kassandra Pb–Zn–Au deposit [10]. The authors identified stibnite (Sb_2S_3) and boulangerite ($Pb_5Sb_4S_{11}$) as the main Sb phases, sometimes occurring together with bournonite and the rare bertherite and valentinite [10]. Our study confirms the abundance of boulangerite, detected through optical microscopy and X-ray powder diffraction analyses. The mineral was present in the form of acicular crystals, and was detected as inclusions within pyrite, galena and within the carbonate gangue of the ores. The close association of boulangerite and galena and the presence of Pb in boulangerite can explain the high Sb concentration observed in the galena concentrate, as most of boulangerite will report to the concentrate at this flotation stage.

The potential recovery of CRMs as by-products, however, is strictly related to mineralogy, texture and mineral chemistry. When CRMs form their own mineral phases, such as Sb in boulangerite and bournonite, the recovery is facilitated. In this case, the separation of a boulangerite concentrate from the galena one can be easily achieved if boulangerite has a sufficiently coarse grain size and can therefore be liberated from the other minerals.

4.1. Boulangerite Content Estimation within Lead Concentrate

Boulangerite crystals were observed both as tiny inclusions in other metallic minerals and as larger crystals in between other phases. The potential for boulangerite recovery from the lead concentrate is related to mineralogy, texture and mineral chemistry. From the antimony content in the lead concentrate (2.06 wt%, Table 3) and the average Sb concentration in boulangerite (25.67 wt%), we can infer that the amount of boulangerite ($X_{bl\text{-}conc}$) within the Pb concentrate was (1):

$$X_{bl-conc} = \frac{2.06 * 100}{25.67} = 8.02\% \quad (1)$$

This result neglects the presence of bournonite and the antimony content which was sequestered in the galena. However, since bournonite has an Sb content very close to that of boulangerite, and very few grains were detected in the samples, we can safely neglect its presence. With regards to the Sb content in the galena, which was 0.32 wt% on average (Table 2), considering that 29.2 wt% of Pb reports to galena concentrate, and that the Pb content of galena was 86.6 wt%, we can estimate first the content of the galena (Xgl-conc) in the galena concentrate (2). This calculation slightly overestimates the antimony amount in galena as we assume that all Pb is galena:

$$X_{gl-conc} = \frac{29.2 * 100}{86.6} = 33.7\% \quad (2)$$

and then the amount of Sb sequestered into the galena crystal lattice ($X_{Sb\text{-}galena}$) (3):

$$X_{Sb-galena} = \frac{33.7 * 0.32}{100} = 0.12\% \quad (3)$$

thus demonstrating that the antimony content within galena can also be safely neglected. Boulangerite (1) is, however, not entirely recoverable. Mineral recovery is widely influenced by physical factors, such as texture, shape, grain size and the wetting properties of the minerals involved. In the next section, we assess boulangerite particle distribution within ore samples through image analysis.

4.2. Boulangerite Particle Analysis

Boulangerite distribution in the samples was quite heterogeneous, with different grain sizes, shapes and modal distributions, which varied from 1% to 17% within the selected back-scattered images (Figure 5). In many cases, boulangerite was detected as

inclusions within other phases, such as pyrite (Figure 5a,b) and galena (Figure 5c). However, boulangerite can also crosscut other minerals (Figure 5d), possibly suggesting that it formed both in earlier and later stages of the mineralization. The use of simple but reliable tools to determine shape factors and the crystal size of these heterogeneously distributed grains is essential for the targeting of the flotation parameters in the separation process.

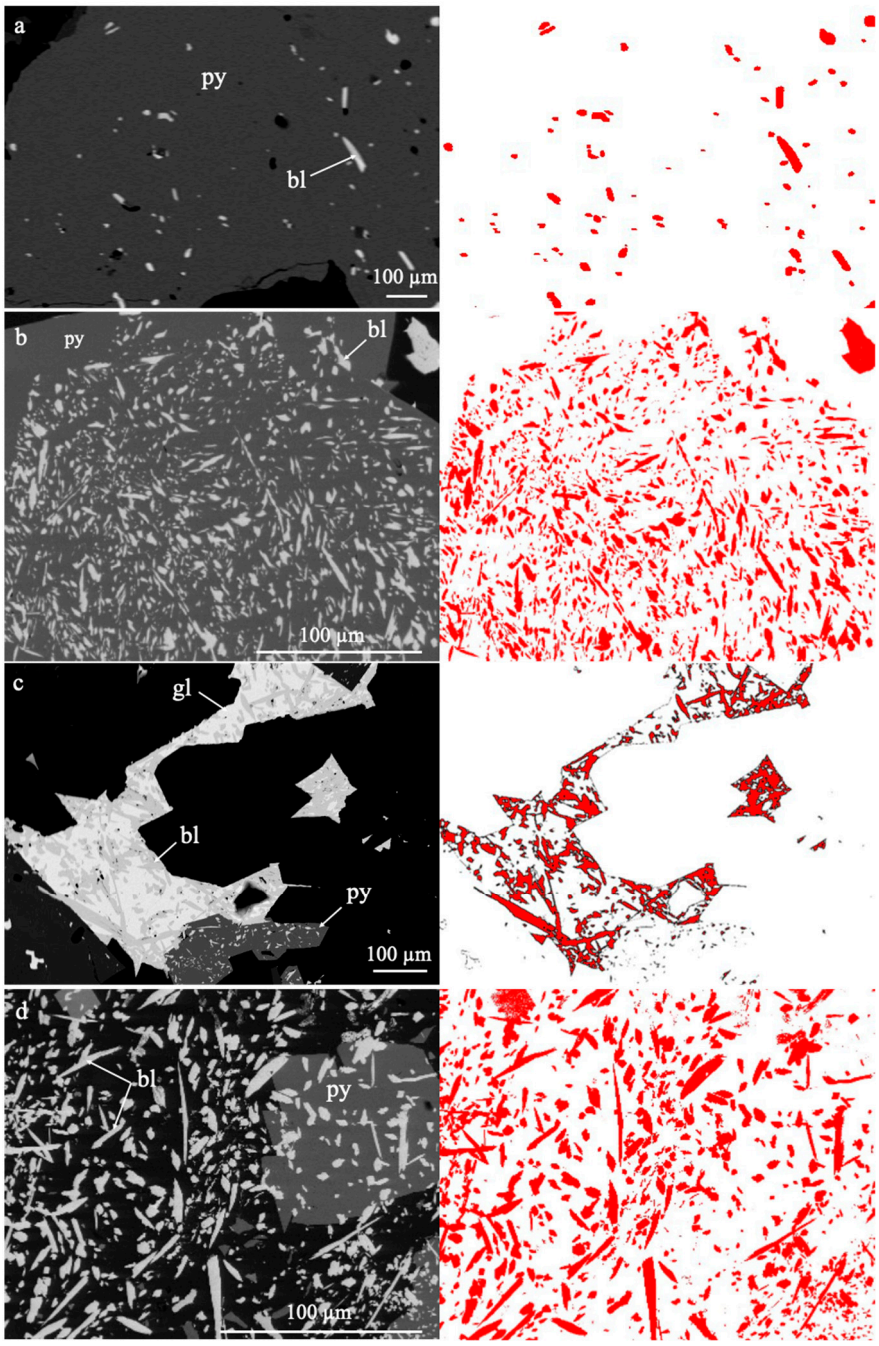

Figure 5. Examples of boulangerite distribution in selected samples; (**a**) rare boulangerite included within pyrite, sample A; (**b**) widespread boulangerite within pyrite, sample C1; (**c**) boulangerite included within galena and pyrite, sample C1; (**d**) boulangerite crystals crosscutting gangue and ore minerals, sample C1.

Boulangerite crystals can cover very different areas if we consider a 2D section. Within eight selected BSE images, covering the full spectrum of detected textures, the total area covered by boulangerite ranges between 1.18 and 24%, with an average of 8.76%, in agree-

ment with the 8.02% of boulangerite in the galena concentrate. Boulangerite areas (μm^2) were divided into the following classes: 0.1–1, 1–10, 10–100, 100–1000 and >1000 (Figure 6). The class with the highest number of particles is 100–1000 μm^2 for one sample (Figure 6a), 10–100 μm^2 for two samples (Figure 6f,h), 1–10 μm^2 for four samples (Figure 6b–e) and 0.1–1 μm^2 for one sample (Figure 6g).

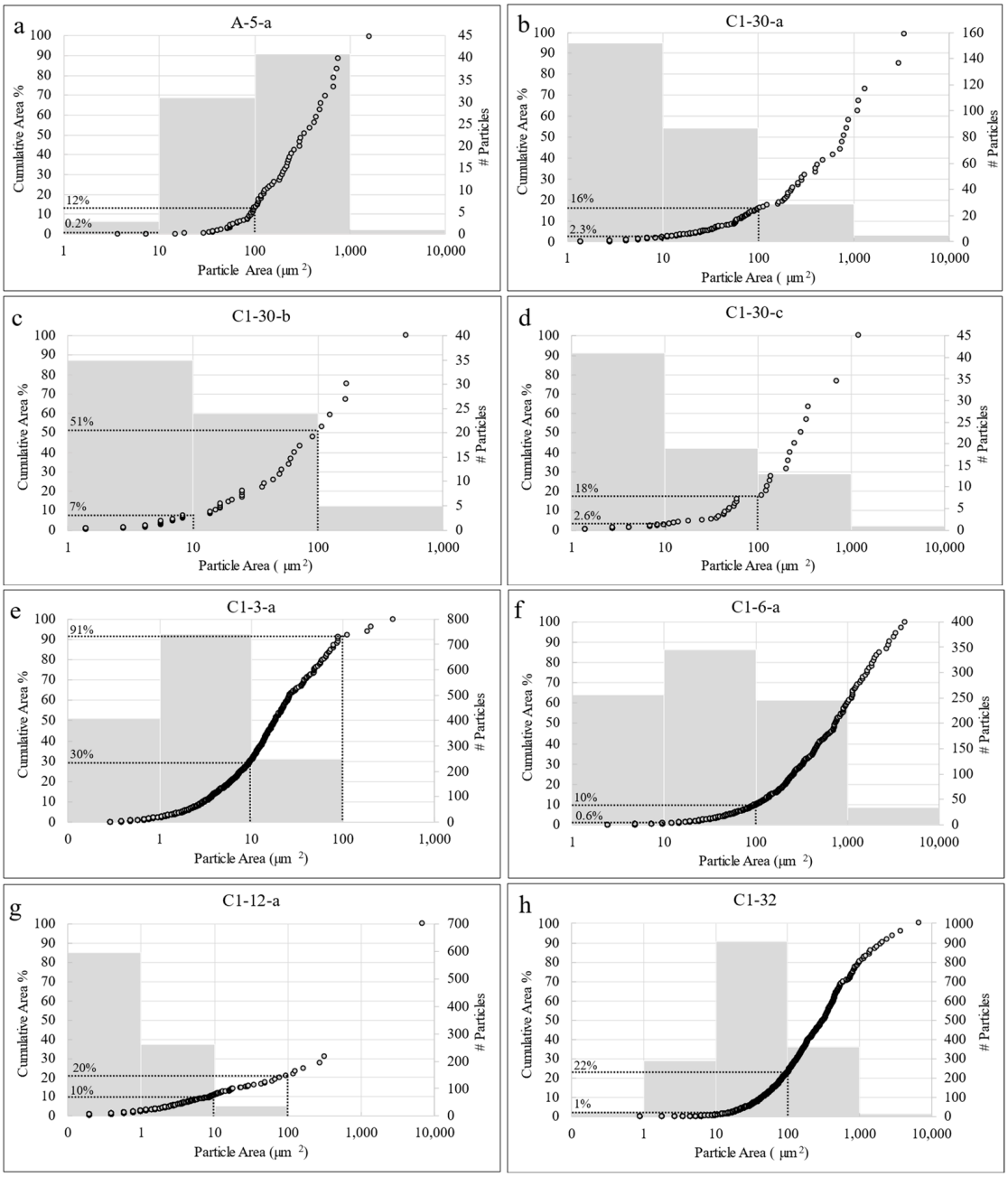

Figure 6. Particle size distribution of boulangerite in eight representative BSE images; cumulative areas of boulangerite particles and frequency of distribution histograms are also reported; ore sample A-5 area a (**a**), ore sample C1, BSE image C1-30 area a (**b**), ore sample C1, BSE image C1-30 area b (**c**) and ore sample C1, BSE image C1-30 area c (**d**), ore sample C1, BSE image C1-3 area a (**e**), ore sample C1, BSE image C1-6 area a (**f**), ore sample C1, BSE image C1-12 area a (**g**), ore sample C1, BSE image C1-32 (**h**).

Despite the predominance of 1–10 μm^2 class grains, the analysis of the cumulative area curve reveals that the particles with an area lower than 10 μm^2 rarely make up for

more than 10% of the total boulangerite area, and in fact it happens only for one section (Figure 6e). This is a positive aspect of boulangerite distribution in terms of separation efficiency through flotation, since particles that are too fine-grained are difficult to liberate and therefore concentrate. This estimation, however, does not consider the shape of boulangerite (as acicular crystals are more difficult to liberate), and the current grain size distribution of the galena concentrate (D50 = 110 μm, Figure 2), which is still too coarse to successfully liberate boulangerite particles with an area close to 10 μm^2. In fact, if we consider a threshold of 100 μm^2 to attain a good boulangerite liberation, about 30% of the total boulangerite would be below this threshold.

Recent enrichment tests on antimony-rich galena concentrates from the Olympias plant [19] showed that antimony could be successfully recovered directly from the galena concentrates through leaching. This one-step beneficiation process involves the use of strongly alkaline sodium sulfide solutions to leach antimony. However, since galena is not affected by the leaching agents, this methodology works best either when boulangerite is not included within other minerals, or when the feed is grinded to a sufficiently small enough grain size to liberate most of boulangerite crystals. Moreover, the treatment of the galena concentrate would involve high amounts of strongly impacting alkaline solutions at the industrial level.

On the other hand, this study proves that since antimony is mostly sequestered in boulangerite, a two-step beneficiation process is not only possible but advisable. Boulangerite can be pre-concentrated from the galena concentrate through froth flotation, and antimony can later be recovered through metallurgical techniques. Boulangerite flotation was studied by Lager and Forssberg [20], who report that the use of ethyl xanthate as a collector agent and pine oil as a frother, alongside the addition of soda as a pH regulator, are the best flotation conditions. The key factor in the two-step process is the boulangerite liberation degree. The current galena concentrate grain size is too coarse to successfully liberate most of the boulangerite, and further tests are needed to pinpoint the optimal grinding degree.

Both in the one-step and two-step processes, mineral chemistry and textural and particle analyses are pivotal to understanding the distribution of antimony in the ores, especially for cases when the metal is mostly sequestered in one mineralogical phase. One-step antimony recovery is possible only when: (i) antimony is enriched within its own mineralogical phase (e.g., the boulangerite for the current case study), and (ii) most of the boulangerite is freed from other minerals (i.e., has a good liberation degree). Therefore, a preliminary particle analysis is necessary, regardless of the chosen concentration technique, to accurately determine the optimal comminution to recover antimony minerals as by-products.

5. Conclusions

The present study shows that the Olympias enrichment plant is a potential sustainable source of antimony for the European Union. The galena concentrate shows a significative enrichment in antimony, mostly in the form of boulangerite. This aspect is favorable for a potential boulangerite recovery, which could be separated from the galena concentrate through froth flotation. Particle analysis on backscattered images of ore samples reveals that the current grain size of the galena concentrate is not suitable to reach a good liberation degree of boulangerite crystals and requires further grinding to a smaller grain size. At the furthest stage of this study, a full evaluation of the degree of liberation was necessary to assess the optimal grain size to achieve a good antimony recovery rate. Upon further grinding, the study showed that the most promising way to produce antimony from Olympias is through a two-step process: (i) a preliminary concentration of boulangerite through flotation, starting from the galena concentrate, followed by (ii) a metallurgical separation of antimony from boulangerite concentrate. The recovery of antimony would provide a new sustainable source of the metal (already considered a Critical Raw Material in the EU) and would simultaneously decrease its contents in mining dumps (thereby decreasing the amount of toxic antimony in the environment). Our findings from the

Stratoni sulfide skarn deposit indicate that similar deposits around Europe could serve as potential antimony targets and could be assessed for future exploitation in further studies.

Author Contributions: Conceptualization, M.B. and G.G.; methodology, A.C. and V.G.; validation, E.T. and V.G.; formal analysis, M.B.; investigation, M.B.; resources, A.C.; data curation, G.G.; writing—original draft preparation, M.B.; writing—review and editing, G.G.; visualization, E.T.; supervision, A.C.; funding acquisition, A.C. All authors have read and agreed to the published version of the manuscript.

Funding: This research received no external funding.

Institutional Review Board Statement: Not applicable.

Informed Consent Statement: Not applicable.

Data Availability Statement: The data presented in this study are available on request from the corresponding author.

Conflicts of Interest: Author Vithleem Gazea was employed by the company Hellas Gold. Author Evangelos Tzamos was employed by the company EcoResources PC. The remaining authors declare that the research was conducted in the absence of any commercial or financial relationships that could be construed as a potential conflict of interest.

References

1. European Commission; Directorate-General for Internal Market Industry Entrepreneurship and SMEs; Grohol, M.; Veeh, C. *Study on the Critical Raw Materials for the EU 2023—Final Report*; European Commission: Brussels, Belgium, 2023.
2. Chakhmouradian, A.R.; Smith, M.P.; Kynicky, J. From "Strategic" Tungsten to "Green" Neodymium: A Century of Critical Metals at a Glance. *Ore Geol. Rev.* **2015**, *64*, 455–458. [CrossRef]
3. Yu, S.; Duan, H.; Cheng, J. An Evaluation of the Supply Risk for China's Strategic Metallic Mineral Resources. *Resour. Policy* **2021**, *70*, 101891. [CrossRef]
4. Henckens, M.L.C.M.; Driessen, P.P.J.; Worrell, E. How Can We Adapt to Geological Scarcity of Antimony? Investigation of Antimony's Substitutability and of Other Measures to Achieve a Sustainable Use. *Resour. Conserv. Recycl.* **2016**, *108*, 54–62. [CrossRef]
5. van den Brink, S.; Kleijn, R.; Sprecher, B.; Mancheri, N.; Tukker, A. Resilience in the Antimony Supply Chain. *Resour. Conserv. Recycl.* **2022**, *186*, 106586. [CrossRef]
6. Anderson, C.G. Antimony Production and Commodities. In *SME Mineral Processing & Extractive Metallurgy Handbook*; Society for Mining, Metallurgy, and Exploration: Engelwood, CO, USA, 2019.
7. USGS. *Mineral Commodity Summaries*; USGS: Reston, VA, USA, 2022.
8. European Commission. *Study on the EU's List of Critical Raw Materials*; European Commission: Brussels, Belgium, 2020.
9. Tzamos, E.; Papadopoulos, A.; Grieco, G.; Stoulos, S.; Bussolesi, M.; Daftsis, E.; Vagli, E.; Dimitriadis, D.; Godelitsas, A. Investigation of Trace and Critical Elements (Including Actinides) in Flotation Sulphide Concentrates of Kassandra Mines (Chalkidiki, Greece). *Geosciences* **2019**, *9*, 164. [CrossRef]
10. Tzamos, E.; Gamaletsos, P.N.; Grieco, G.; Bussolesi, M.; Xenidis, A.; Zouboulis, A.; Dimitriadis, D.; Pontikes, Y.; Godelitsas, A. New Insights into the Mineralogy and Geochemistry of Sb Ores from Greece. *Minerals* **2020**, *10*, 236. [CrossRef]
11. Bussolesi, M.; Zaccarini, F.; Grieco, G.; Tzamos, E. Rare and New Compounds in the Ni-Cu-Sb-As System: First Occurrence in the Gomati Ophiolite, Greece. *Period. Mineral.* **2020**, *89*, 63–76. [CrossRef]
12. Himmerikus, F.; Reischmann, T.; Kostopoulos, D. Triassic Rift-Related Meta-Granites in the Internal Hellenides, Greece. *Geol. Mag.* **2009**, *146*, 252–265. [CrossRef]
13. Siron, C.R.; Rhys, D.; Thompson, J.F.H.; Baker, T.; Veligrakis, T.; Camacho, A.; Dalampiras, L. Structural Controls on Porphyry Au-Cu and Au-Rich Polymetallic Carbonate-Hosted Replacement Deposits of the Kassandra Mining District, Northern Greece. *Econ. Geol.* **2018**, *113*, 309–345. [CrossRef]
14. Karin Högdahl1, E.J.S.R. Ore Mineralogy, Trace Element Distribution and 3D X-ray Tomography of the Polymetallic Sulphide Deposits at Mavres Petres and Piavitsa, Greece. In Proceedings of the 15th Biennial SGA Meeting, Glasgow, UK, 27–30 August 2019; pp. 27–30.
15. George, L.; Cook, N.J.; Ciobanu, C.L.; Wade, B.P. Trace and Minor Elements in Galena: A Reconnaissance LA-ICP-MS Study. *Am. Mineral.* **2015**, *100*, 548–569. [CrossRef]
16. Renock, D.; Becker, U. A First Principles Study of Coupled Substitution in Galena. *Ore Geol. Rev.* **2011**, *42*, 71–83. [CrossRef]
17. Cook, N.J.; Ciobanu, C.L.; Pring, A.; Skinner, W.; Shimizu, M.; Danyushevsky, L.; Saini-Eidukat, B.; Melcher, F. Trace and Minor Elements in Sphalerite: A LA-ICPMS Study. *Geochim. Cosmochim. Acta* **2009**, *73*, 4761–4791. [CrossRef]
18. Frenzel, M.; Hirsch, T.; Gutzmer, J. Gallium, Germanium, Indium, and Other Trace and Minor Elements in Sphalerite as a Function of Deposit Type—A Meta-Analysis. *Ore Geol. Rev.* **2016**, *76*, 52–78. [CrossRef]

19. Megaloudi, R.A.; Kourtis, A.; Oustadakis, P.; Tzamos, E.; Dimitriadis, D.; Xenidis, A. Antimony Extraction from Galena Concentrates. *Mater. Proc.* **2022**, *5*, 130. [CrossRef]
20. Lager, T.; Forssberg, K.S.E. Beneficiation Characteristics of Antimony Minerals a Review—Part 1. *Miner. Eng.* **1989**, *2*, 321–336. [CrossRef]